High Power Terahertz Light: Commissioning and Characterization

A thesis submitted in partial fulfillment of the requirement
for the degree of Bachelor of Science in
Physics from the College of William and Mary in Virginia,

by

Amelia Seleste Greer

Advisor: Dr. Gwyn P. Williams

Williamsburg, Virginia
Mary 2006

Abstract

THz light, with a frequency of 10^{12} Hz does not occur naturally at a high enough intensity to study. The electron accelerator at the Free Electron Laser at Jefferson National Accelerator Facility, however makes 100 Watts of THz light, which is bright enough to study. This research project involved the commissioning and characterization of this light. Specifically, it involved the alignment of the beam transport for the light, and the thorough analysis of the machines and their noise which will be used to help study the THz light in the future.

Acknowledgements

I would like to thank my advisor, Dr. Gwyn P. Williams for being my mentor in research and Physics during the last two years. His guidance, knowledge and kindness have given me invaluable experience working in a lab and the rare opportunity, as an undergraduate to be a part of cutting edge physics research. It has been a thrilling experience for which I am infinitely thankful.

I would also like to thank Dr. Michael Klopf for his patience in explaining the detailed physics behind the research and willingness to lend a helping hand and give guidance throughout the second half of my research and the writing of this report. In addition, I would like to extend thanks to Rich Evans and Pavel Evtushenko along with everyone else at the FEL for their continuous help and for giving me the opportunity to work with such a great team.

Table of Contents

1. Introduction

1.1. Introduction to THz

Jefferson National Accelerator Facility (Jlab) has two particle accelerators. The Terahertz (THz) project at Jlab centers around the accelerator for the Free Electron Laser (FEL), which makes 100 Watts of THz light. This is 10^5 times brighter then any other source in the world up to this point. THz Light has a frequency of 10^{12} Hz, placing it between microwaves and visible light in the far-infrared range of the electromagnetic spectrum. On the electromagnetic spectrum, THz falls between electronics and photonics. Figure 1 shows where THz lies, with the blue line being the electromagnetic spectrum.

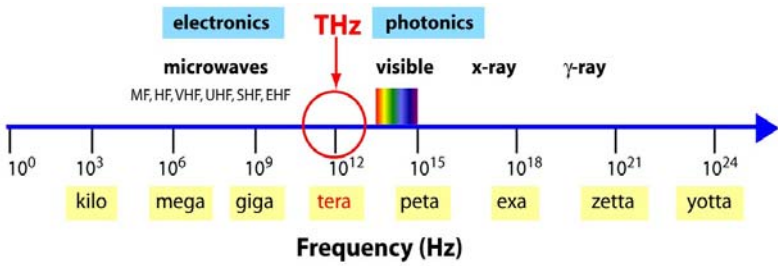

Figure 1. Chart shoring the electromagnetic spectrum, with different frequencies along the blue line. This diagram shows that THz light lies at 10^{12} Hz between electronics and photonics.

This is a part of the spectrum that we knew little about until recently; up until now we haven't really been able to study it due to lack of intensity. We are learning however, that THz lies in an important area as far as understanding fundamental properties of material, for example conductors, semi-conductors, and protein dynamics. THz is also non-ionizing and matches the vibrational energies of molecules and atoms in solids

allowing us to study them in great depth. These unique properties can lead to a wide range of uses.

1.2. Introduction to the Applications of THz

1.2.1. THz Applications in Defense

One of the major applications of THz, imaging, has great potential to help out in the field of defense, among other things. THz interacts weakly with things like paper, cloth, and walls. This property can be used to improve concealed weapon detection. Figure 2 (a) shows a photograph of a fully clothed man, holding a newspaper. Figure 2 (b) shows an image of the man in which you can see through the paper and the clothing to reveal that he is concealing a knife under the paper and a gun under his clothes, on his hip.

(a) (b)

Figure 2. Photograph showing a man fully clothed and holding a newspaper in (a) and an image of the same man taken in cm waves which reveals a knife under the newspaper and a gun on his hip in (b).

The image in Figure 2 (b) is actually taken using centimeter waves. If the image were in THz you would be able to see more detail, smaller weapons and even plastic explosives. This is made clear in Figure 3 (a) which shows an actual THz image of a

shoe from below. This image shows a concealed ceramic knife in the toe and plastic explosives in the heal. Figure 3 (b) shows a photograph of the cross-section of the actual shoe with the sole removed. There is a much higher level of clarity in the THz image, shown in Figure 3 (a), then in the image, in Figure 2 (b), taken in centimeter waves.

(a) (b)

Figure 3. THz image of a shoe revealing a hidden ceramic knife in toe and plastic explosive in heal in (a) and photograph showing the same shoe with sole removed in (b).

In addition to images that can help with hidden weapon detection, THz light can help to identify and distinguish between different types of explosives. Figure 4 shows several different spectra. Each explosive has a different "Terahertz spectral fingerprint" (TeraView). This means that not only can the THz detect the presence of an explosive, but it can also determine which explosive it is. One advantage of this is that with the knowledge of the specific explosive, it can then be handled accordingly.

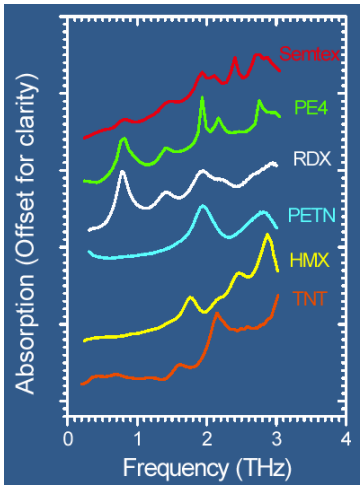

Figure 4. The spectra of several different explosives taken using THz.

1.2.2. THz Applications in Biomedicine

THz light also has vast potential for scientific improvements in biomedical fields. In dentistry, for example, images can be taken of teeth that clearly outline the conditions of the different layers, exposing missing enamel or cavities. Figure 5 (a) shows an image composed from absorption data of a tooth. The pink area is the location of a cavity. The photograph of the tooth exterior is shown in Figure 5 (b). From the photograph in Figure 5 (b) very little can be told about the tooth, but with the THz image in Figure 5 (a) a great deal can be learned without removal or x-rays.

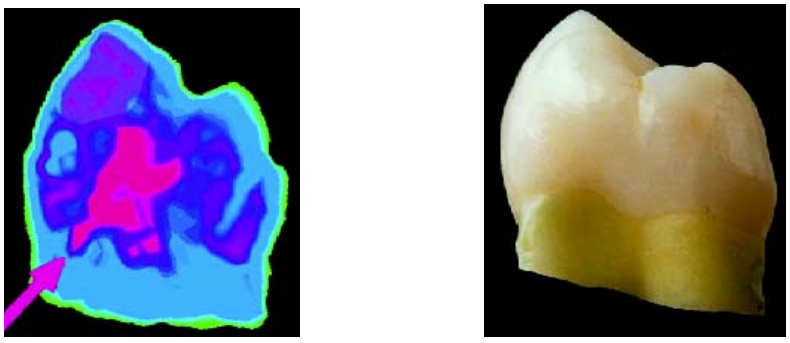

(a) (b)

Figure 5. THz image of a tooth showing location of a cavity in pink in (a) and photograph of the same tooth in (b).

In addition to dental imaging, THz imaging has great potential to improve the detection of different types of cancer. Because the light interacts strongly with water we cannot yet detect cancers below the surface. However someday, we may be able to with the help of fiber optics or other transport systems which would allow us to get the light deeper into the body. For the time being, though, it can be used to help detect oral cancers and basal cell carcinoma (skin cancer).

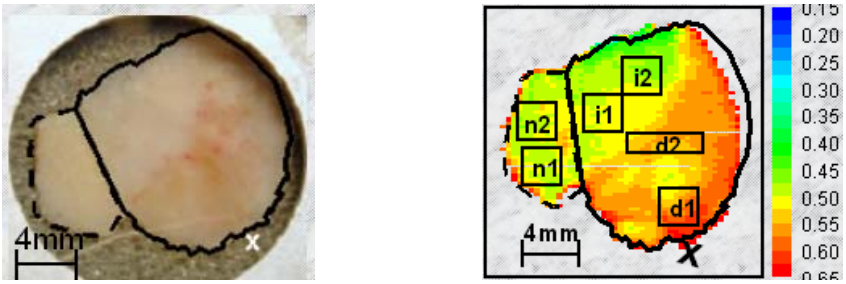

(a) (b)

Figure 6. Photograph of skin imperfection in (a) and THz image of same imperfection showing cancerous region in red in (b).

A close-up photograph of a skin imperfection is shown in Figure 6 (a). The THz image is shown in Figure 6 (b). The red region in Figure 6 (b) shows the cancerous area. The future hope is that an entire person's body could be scanned to reveal all potential problem areas. These informative images can help to eliminate the amount of times a cancerous spot will have to be operated on. Instead of removing small areas and then testing and repeating until the area is no longer malignant, THz would allow surgeons to know exactly where the cancer lies so that one operation would be sufficient. There is hope that this would vastly improve the method for removing breast cancer in addition to treating skin cancer. These THz images, though unable to give the complete picture of a person and their ailments, are complementary to and can be very helpful in combination with MRI and x-ray.

Despite all of its valuable applications, THz light has not really been used on a large scale (up until now). This is due to its lack of intensity in everyday life. In order to become intimately familiar with this problem of intensity, it's helpful to attempt to use THz. In other words, by learning where the problem arises, it is then easier to understand how to fix it. This can be done, in part, through infrared spectroscopy.

1.3. Introduction to Spectroscopy

Due to the fact that THz hasn't been studied in a great deal of depth until recently, it is useful to begin a study of spectroscopy in the mid-infrared range. Then, the knowledge acquired from this range can be applied to the far-infrared range, where THz is located. The machine used for this purpose was a Nicolet spectrometer in combination with OMNIC 5.1 computer software to control the machine. The spectrometer follows the layout of a typical Michelson interferometer. Figure 7. shows a schematic of the spectrometer used. The mid-infrared source light comes from the spot labeled point (for point source). Then the light hits an ellipsoidal mirror which focuses it and then sends it to a parabolic mirror. The parabolic mirror collimates the light and sends it through a beam splitter where half of it goes to the movable mirror and half of it goes to the fixed mirror. Then the two beams recombine and go on to a parabolic mirror to focus them again and then they hit one more ellipsoidal mirror before going into the detector. In order to test some sample material in the machine, the sample would be placed between the last parabolic and ellipsoidal mirrors.

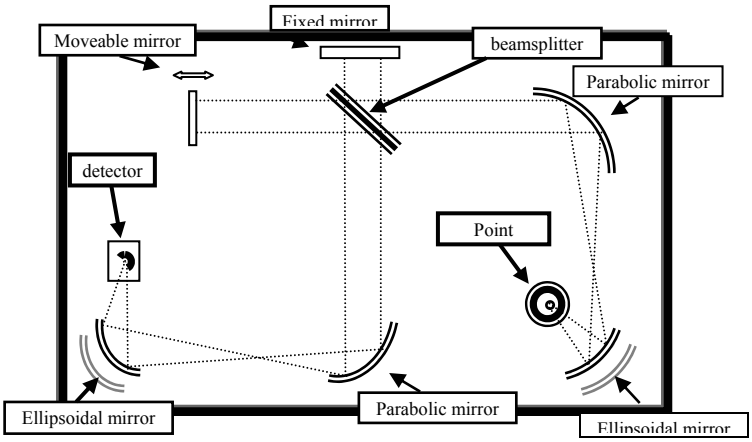

Figure 7. Schematic showing the components and approximate layout of the Nicolet Spectrometer used in this research.

The movable mirror pictured in the upper left corner could be set to scan a certain number of times. The resolution of the machine was also adjustable. The resolution is determined by the length traveled by the movable mirror in the machine. Using OMNIC through a desktop computer, the parameters on the machine could be altered in order to become familiar with the spectrometer, analyze the machine, and in the process learn more about THz.

The noise is one issue that must be acknowledged on any machine, including the Nicolet spectrometer. The equation for noise can be given as

$$\%N = \frac{100 \cdot A^{\frac{1}{2}} \cdot D^*}{\phi(\upsilon) \cdot \varepsilon \cdot \xi \cdot \Delta\upsilon \cdot t^{1/2}} \qquad (1)$$

where %N is the percent noise. The area of the beam is given by A, the detectivity of the spectrometer is D*, $\phi(\upsilon)$ is the brightness of the source, ε is the aperture, and ξ is the optical efficiency. $\Delta\upsilon$ represents the bandwidth, or in the calculations done for this research, the resolution, and the time, or the number of scans, is given by t.

Equation (1), shown above, can be rearranged so that all the adjustable parameters, the resolution, the number of scans and the noise which changes as a result of those, are on one side of the equation. The remaining parameters should be a constant, since they are a built-in part of the machine, and thus we assume them to be unchanging. Then the "adjustable" parameters are set equal to the "constant" parameters. The resulting rearranged equation, equation (2) is as follows:

$$\%N \cdot \Delta\upsilon \cdot t^{1/2} = \frac{100 \cdot A^{1/2} \cdot D^*}{\phi(\upsilon) \cdot \varepsilon \cdot \xi} = \text{constant} \qquad (2)$$

with all of the components representing the same elements as those in equation (1). Using this new equation, the "constant" can be calculated for different spectra. One aspect of the spectrometer examined, was the effect of setting the resolution at 0.25, 0.50, 1.0, 2.0, 4.0, 8.0, and 16.0 wavenumbers. Where a wavenumber is 1 over the frequency in cm. Another aspect was to look at the varying results with 1, 2, 4, 8, 16 and 64 scans. With this data, the constant for the various resolutions could be compared to the scans vs. the resolution, the number of scans and the length of time the data collection itself took could be shown on a graph. An example of one of these graphs is shown in Figure 8. This graph shows the resolution versus the constant calculated at 1, 2, 4, 8, 16 and 64 scans. The lower the constant, the lower the noise and therefore the more desirable the setting.

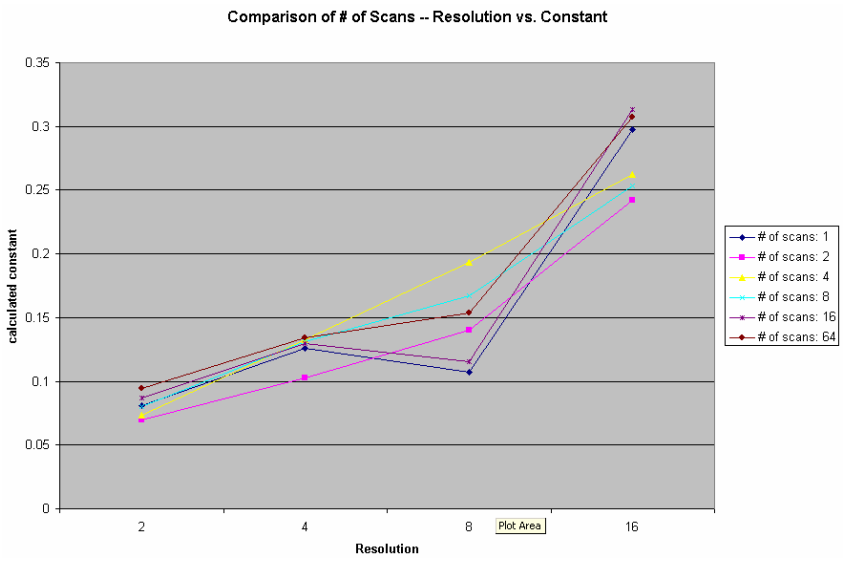

Figure 8. Graph showing the resolution versus the constant at 1 (marked by the dark blue diamond), 2 (marked by the pink square), 4 (marked by the yellow triangle), 8 (marked by the light blue arrows), 16 (marked by the purple stars) and 64 scans (marked by the brown diamond).

This graph shows that the lower the resolution, the worse the constant. The lowest resolution on the graph is 16 wavenumbers and the highest resolution is 2 wavenumbers. This may seem slightly surprising, as it is often thought that the noise increases as the resolution increases. A possible reason for this opposite result is vibration of the moveable mirror. As the resolution decreases, the movable mirror ends up vibrating because it is making shorter scans and taking less time. As a result of this, the optical efficiency, which I assumed constant, is actually changing, and thus the noise and the calculated constant is increased.

When the spectrometer is adjusted to look at the THz, far-infrared region, the noise dramatically increases. Figure 9 shows a sample percent transmittance. The less noise there is at a certain frequency the straighter the line at that point. The noise "explodes" in Figure 9 (a) as it approaches the THz region on the right side. In other words, the noise goes up greatly in the THz range. Figure 9 (b) is a zoomed in version in

which the noise for that section can be seen. When evaluated by the machine, the noise in that area is shown to be almost 200 percent in contrast to the 0.2, 0.1, 0.01 percent found in the mid-infrared region previously. For reference, 1 THz is equal to 33 wavenumbers which can be seen clearly in Figure 9 (b).

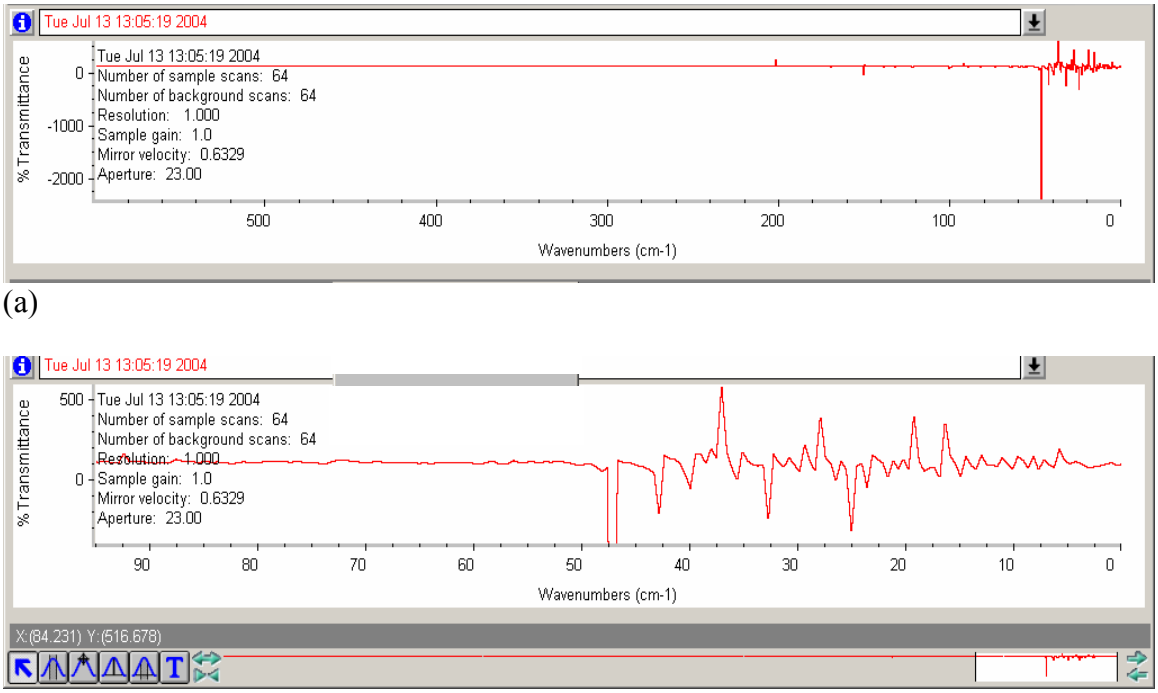

Figure 9. Percent transmittance showing the increasing noise in the THz range of frequencies on the right side of (a) and a zoomed in version of the THz region in (b).

Since a percent noise of 200 makes any data useless, the lack of THz use until recently is easy to understand.

Reexamining the noise equation (1) from earlier, where the brightness, $\phi(\upsilon)$, is in the denominator, it is clear that increasing the brightness of the source would significantly decrease the noise. This is precisely what is done with the Free Electron Laser (FEL) at Jefferson Lab. Figure 10 shows a graph illustrating how much more intensity (also known as brightness) we can get from the light made at the FEL. The

green line is the brightness level achieved by synchrotron emission generally for different frequencies. The x-axis shows the frequencies from left to right going from small to large (the opposite orientation of the x-axis shown in Figure 9 (a) and (b)). That is, the THz region is located on the left half of the graph. The blue line then shows the level of brightness that can be achieved at the FEL. This graph illustrates that the enhancement at low frequencies (i.e. in the THz range) is proportional to the square of the number of particles, N^2, in each electron bunch. At the FEL, N is typically on the order of 10^8.

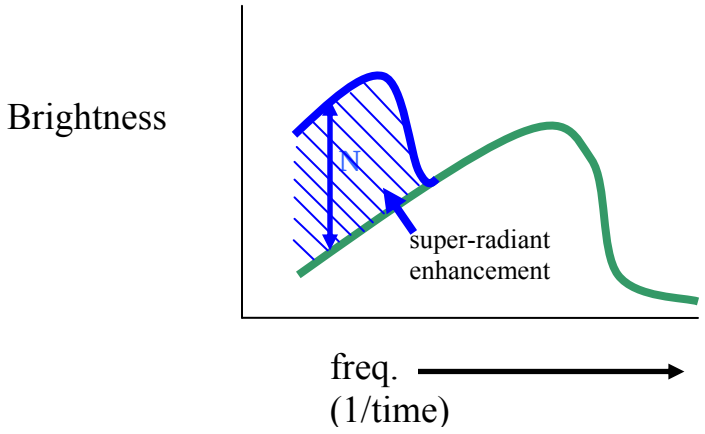

Figure 10. Graph showing the increased brightness level achieved by the FEL (in blue) compared to that generally achieved by synchrotron emission for different frequencies (in green).

1.4. Introduction to the THz Beamline

In Figure 10, above, you can see that the FEL accelerator at Jefferson lab can produce high power THz light. However, the accelerator is located, and the light is made, underground in a radiation shielded vault. No one is allowed in this vault while the accelerator is on, and thus while the light is being made. In order to have access to the THz, it is necessary to convey the light into a lab where it can be studied. This is done using what is known as a beamline. The beamline is a transport system that

transmits the light from underground, in the vault in the FEL to the second floor of the building and into a lab using a series of 4 mirrors. A drawing of the beamline is shown in Figure 11.

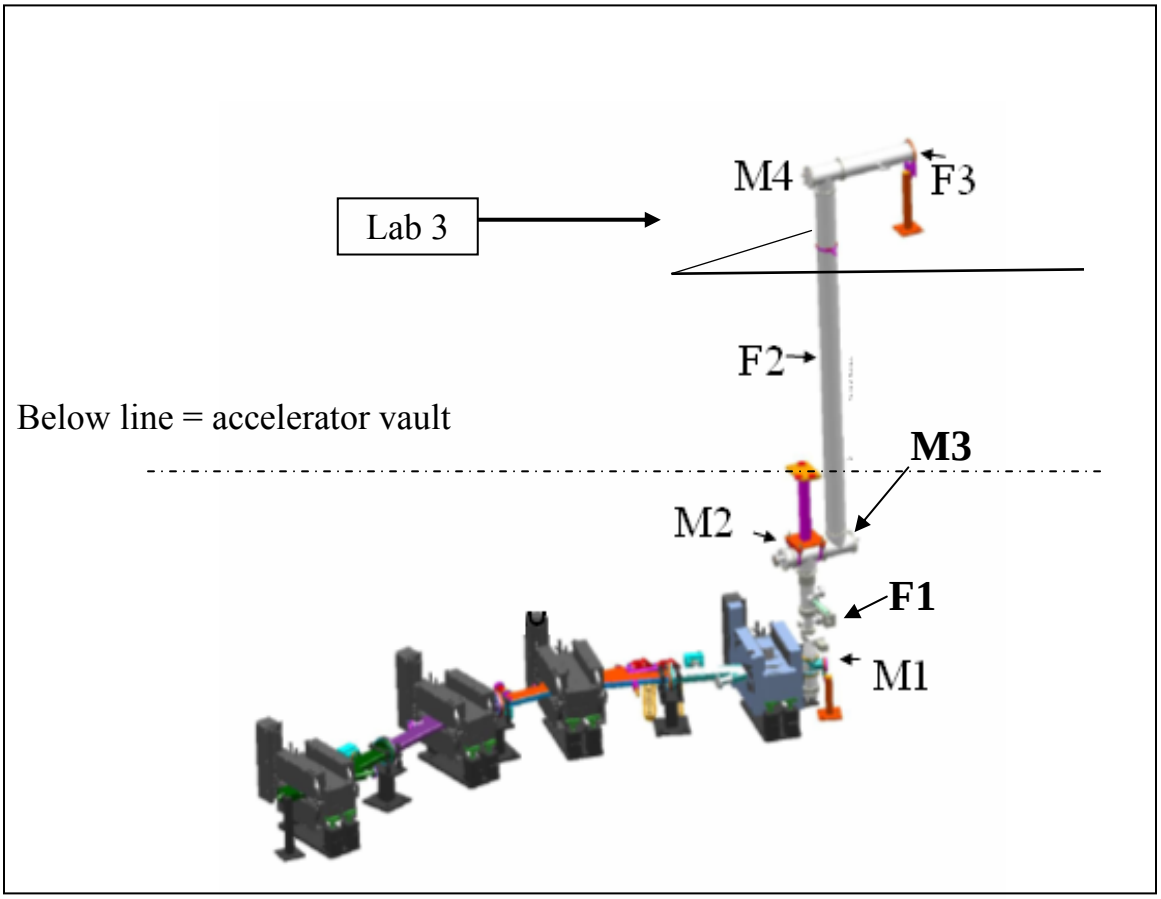

Figure 11. Schematic showing the beamline and the location of the four mirrors and three diamond windows.

I helped to assemble and to test the four mirrors and mirror mounts that make up the beamline. One of the mirrors is shown schematically in Figure 12 (a). Figure 12 (b) is a photograph of the first in the series of mirror mounts and mirrors which I assembled.

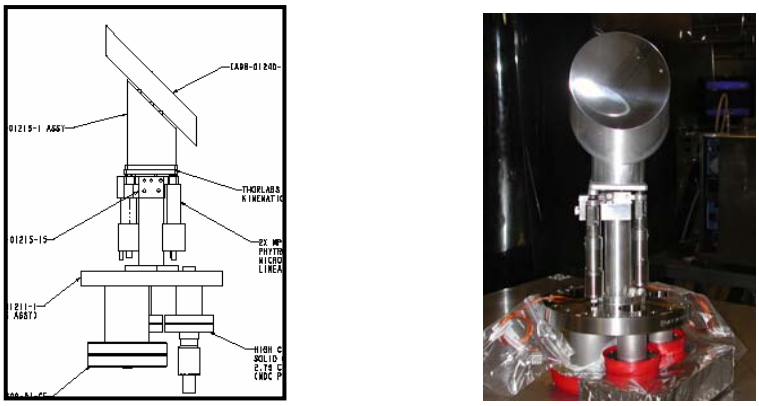

(a) (b)

Figure 12. Technical drawing showing M1 in (a) and photograph of assembled M1 in (b).

2. Commissioning:

This section of the research entails the installation and alignment of the THz beamline in the FEL. During my research at Jlab and in particular this part of my focus, I have worked closely with Gwyn Williams, Michael Klopf, and several other members of the FEL team. It would be a difficult task to work on this project solo, and at large labs, in general, people work in groups. Working in this fashion was an important part of my experience with this project.

In the FEL building at Jlab, whenever the Free Electron laser is running it is referred to as "beam on." Since no one is allowed in the underground vault where the accelerator is located during this time, we had to wait until the beam was not running. During one such time, we were able to go into the vault and work on the beamline alignment. First, the spool located above the F1 diamond window was removed in order to allow access to M1 (F1 and M1 both shown in Figure 11). Then a diode back-tangent alignment laser (DBT) was set up in a position such that it hit M1 approximately 1 cm off the center of the mirror surface. We, then, adjusted M1 to direct the DBT beam through the center of the diamond window. When observed, two spots of light showed. We

figured that this was likely due to multiple reflections in the DBT laser input window (which was later found to be true). Taking this into consideration, we aligned the brightest spot of light to be in the center. Following this, we shifted M2, in order to place the DBT laser slightly off-center, in the same direction as M2, on M3. Then M3 was adjusted so that the DBT was slightly off-center on M4 and M4 was positioned such that the DBT beam went through the center of the diamond window located at F3. When we placed a 1mm aperture at F1, we found that the DBT beam imaged well at F3. Then to run another check, we placed a small maglight bulb at F1 and found that it too imaged well at F3. Following this, we ran yet another test for alignment by removing M4 and checking to see if the image from the bulb was centered in the beamline chamber. It was, so we then replaced M4, and using 2 apertures in the lab, examined the beam as it came out of the beamline. Placing a 1mm aperture at F3, we were then able to adjust M4 to maximize the brightness of the beam and align the beam parallel to the optical bench where experiments will be located in the lab. And finally, a HeNe alignment laser in the THz hutch was aligned so that its beam was co-incident with the beam of the DBT and the spool above F1 was replaced. This concluded the alignment of the beamline mirrors and diamond windows for the time being.

3. Characterization

This portion of my project allowed me to focus on the tools for analyzing and evaluating the THz light and the analysis itself. This involved three parts—the spatial extent of the beam and the focusing qualities of the beamline optics, the absolute power, and the spectrum.

3.1. Spatial Extent of the THz Beam

This was a continuation of the earlier alignment procedures, only with real THz beam instead of a small alignment laser, and an Infrared camera instead of merely visually studying images. Figure 13 (a) shows an image of the beam taken by Mike Klopf with the infrared camera. Figure 13 (b) is an image created from calculations done by Paul Dumas, Oleg Chubar and Gwyn Williams. Figure 13 (b) shows interference fringes because the calculation was done for a single wavelength of THz, however the shape is very similar to the image in (a). Note that both have a triangular shape. This comes from the asymmetry in the production mechanisms. This is exciting because it shows that the actual image agrees with the calculations and thus the beamline and accelerator work as expected.

(a) 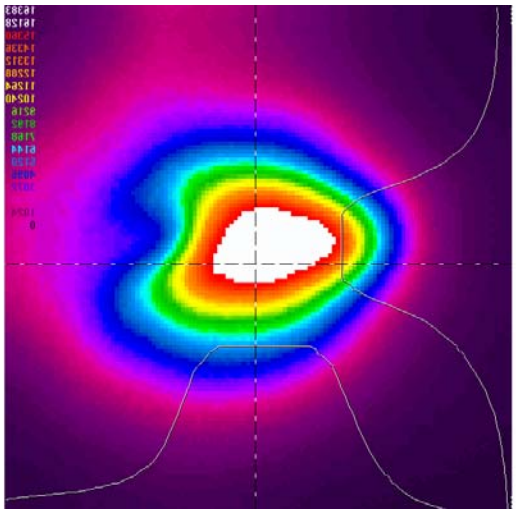 (b) 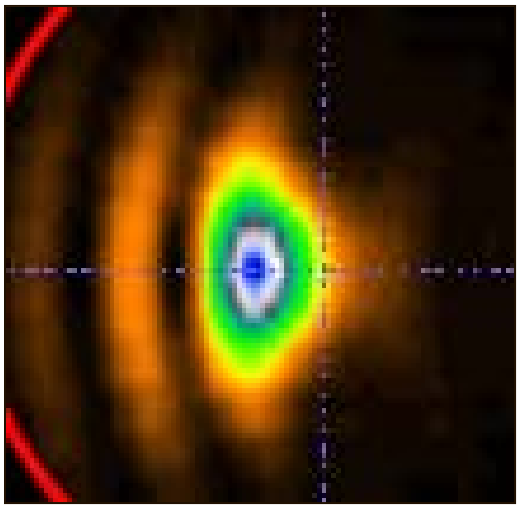

Figure 13. Image showing THz beam, taken by Michael Klopf, in (a) and image created from calculations by Paul Dumas, Oleg Chubar and Gwyn Williams in (b).

3.2. Power Measurement

I only worked with the Absolute Power/Energy Meter in theory. The absolute power meter is based on measuring the acoustic wave generated by a metal film that absorbs a known fraction of the beam. For this, the beam has to be chopped. The acoustic wave is then compared to the one produced by an electrical impulse in the same film. The absorption can be shown in the following calculations by Larry Carr at Brookhaven:

$$\text{Absorption} = \frac{(4 * 377 / \text{Rfilm})}{[(377 / \text{Rfilm}) + n + 1] * 2} \tag{3}$$

where Rfilm is the resistance of the film being used, n is the refractive index and 377 is the permittivity of free space. This equation works assuming a homogeneous, dirty (alloy) metal film. This means that the calculations are frequency independent and that you can get 50% absorption only when there is no substrate, or in other words, if the film is freestanding. The maximum absorption can be written:

$$A_{max} = \frac{1}{(n + 1)} \tag{4}$$

This comes from the fact that the absorption has its maximum when

$$\text{Rfilm} = \frac{377}{(n + 1)} \tag{5}$$

Figure 14 shows the Absorption, Transmission and Reflection for a free standing film as a function of the sheet resistance, with the sheet resistance in Ohms/cm^2. Notice

that the Transmission and the Reflection only intersect when the absorption is at its maximum. This is only the case when there is no substrate, i.e. n = 1.

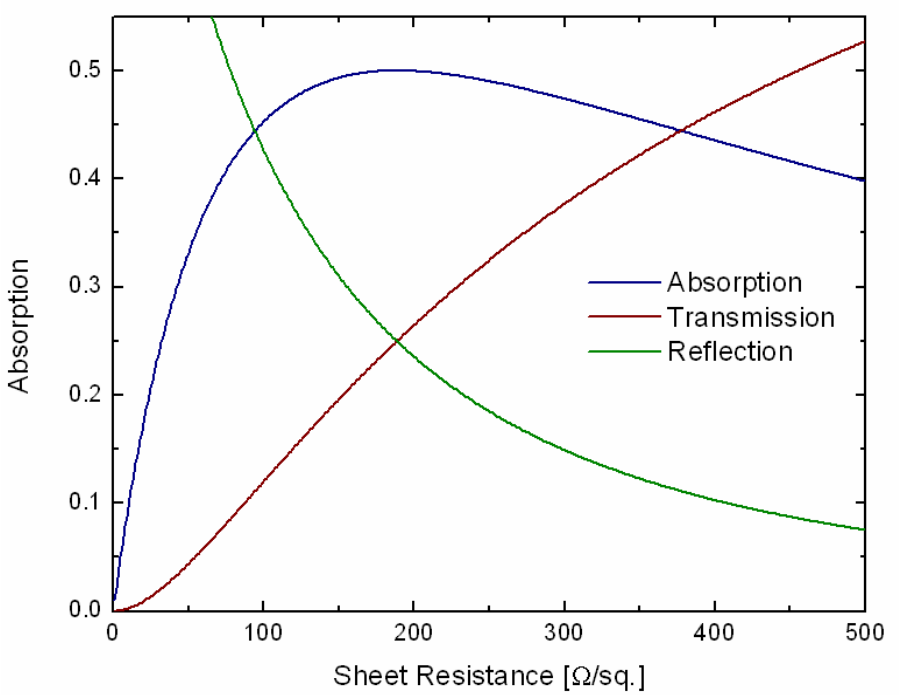

Figure 14. Graph showing the absorption, transmission and reflection for a free standing film as a function of the sheet resistance.

3.3. Spectroscopy In-Depth

3.3.1. Gaining a Better Initial Understanding of the Nicolet Spectrometer

In the first part of my research I worked closely with the Nicolet Spectrometer and furthered my understanding of the basic machine, how it works, the intricacies of the OMNIC software that runs it, and gained more insight into the output data. I began by working with Richard Evans, a long time, experienced employee of the FEL program, currently working on his masters in applied physics at Christopher Newport University. With his general knowledge, and my previous experience with the spectrometer, we began probing the deeper understanding of the components of the machine and the OMNIC program. After working together to further both our understandings, we

separated to focus on our own specific interests. Rich's task was to move the spectrometer into a vacuum chamber and modify the electronics to accommodate the change, while mine, in respect to the spectrometer, was to characterize the new set up of the spectrometer and verify the operation of it. This was done successfully and the method is elaborated upon further, later on.

3.3.2. Return to Reproducibility

I took several spectra to test the reproducibility. I collected data at a resolution of 4, with 1 scan, 4 scans, 64 scans and 128 scans. In order to get the spectra, the machine first takes a background spectra at the settings you've told it, and then takes a second at the same settings. Then OMNIC compares the two. If there is no noise, or relatively little noise, the result should look roughly like a straight line. This then allows us to see the reproducibility, i.e. how reproducible the spectra are at certain settings of the machine. The less a spectra is like a straight line, the more noise it has. In Figure 15, all of the lines were taken at a resolution of 4. The red line was taken at 1 scan. The dark blue line was taken at a setting of 4 scans. The pink line is at 64 scans and the green line is at 128 scans. The lines appear to decrease in noise as the number of scans increases, until 128, where it appears to be slightly less clear than the spectra taken at 64 scans. This may be due to a problem similar to one I discussed earlier, that of optical efficiency. As the machine has to do more and more scans, the scanning mirror may begin to vibrate, decreasing the optical efficiency and increasing the noise.

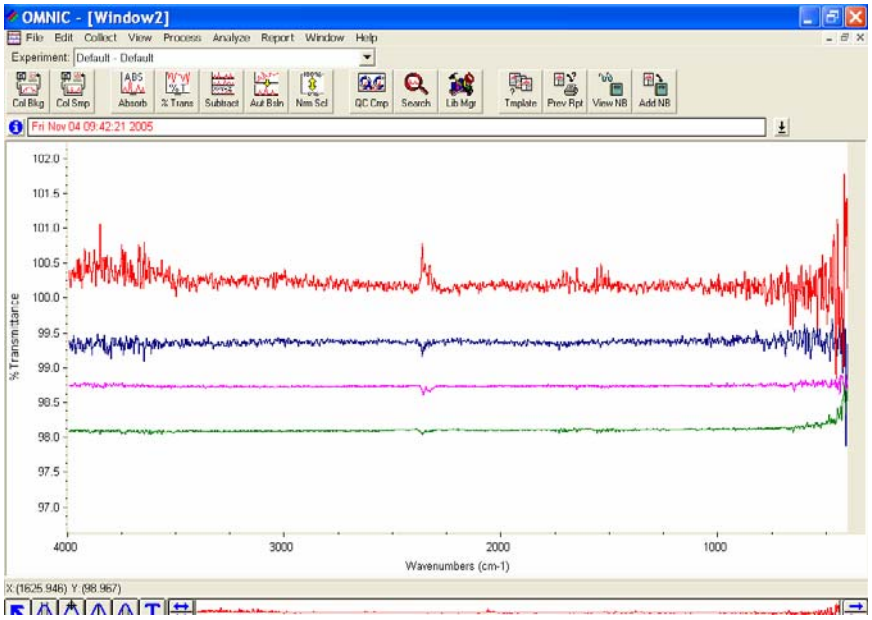

Figure 15. Image showing percent transmissions taken at a resolution of 4. The red line was taken at a setting of 1 scan, the blue was taken at 4 scans, the pink was at 64 and the dark blue was taken at 128. Note, the large amount of noise on the right hand side is likely due to low signal at those frequencies which mean that when the percent transmission is taken (by dividing one spectra by another one) you may end up dividing by approximately zero.

In addition to testing the reproducibility, I also took data to demonstrate the resolution. Figure 16 pictures four background scans taken at 64 scans with varying resolution settings, where the resolution is in wavenumbers. The red line was taken at a resolution of 16. The dark blue line was taken at a resolution of 4. The pink line was taken at a resolution of 1 and the green line was taken at a resolution of 0.25.

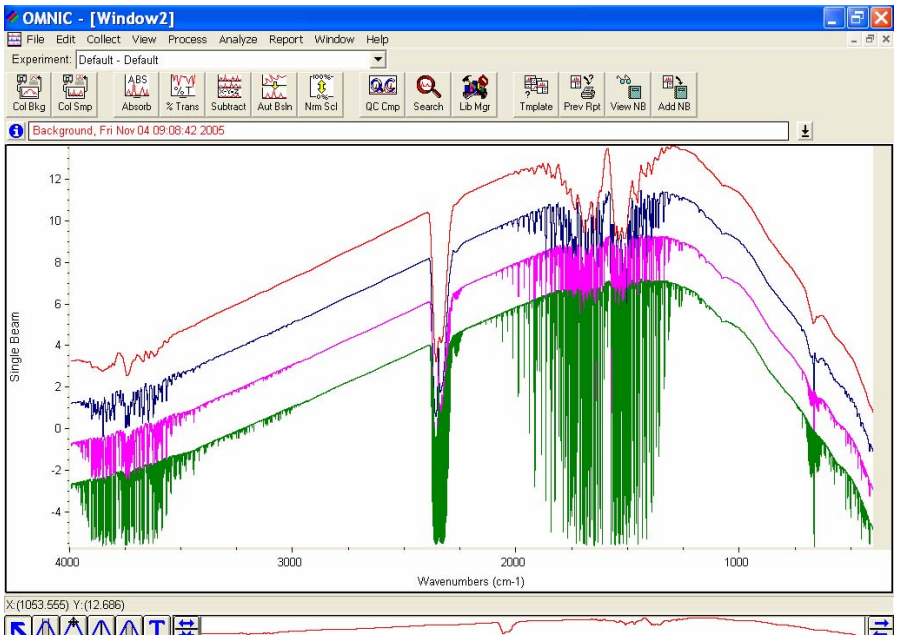

Figure 16. Image picturing four background scans taken at 64 scans with different resolutions. Red is taken at a resolution of 16 wavenumbers, dark blue is at 4 wavenumbers, pink is at 1 wavenumbers and green is at 0.25 wavenumbers.

3.3.3. Vacuum Spectrometer

As mentioned previously, THz is strongly absorbed by water, and thus water vapor which is present in a relatively high, varying amount in the air around us. Because of this, using THz in a spectrometer not in vacuum could lead to poor results. However, since THz is still very new on this large scale, there are few instruments designed for this purpose. In order to get around this problem, the internal components of the Nicolet Spectrometer were removed from the original casing and placed in a custom made box designed for vacuum by Gwyn Williams. This box will ultimately be a vacuum chamber though as of now it is still waiting on other pending aspects of the THz project.

Despite the new outer casing, the machine is still operated through the aforementioned computer program, OMNIC 5.1. Though the physical transfer of the

components went smoothly, getting the relocated Nicolet to run as it had before proved more difficult.

The first step was to ensure that the computer interface was connected appropriately and to test it. When we did this, we found that the alignment laser was off. This meant that the machine had trouble taking any sample data. After aligning the laser, we again tried to run the machine. However, we found that even with our new alignment, the machine ran very slowly and seemed to struggle with the data taking process. To remedy this, a Nicolet technician came to check everything and ensure that the system was aligned properly and working smoothly in the machines new configuration.

3.3.4. Testing the Vacuum Spectrometer

From this point, I began testing the new machine. It was important to make sure that the "new" machine would operate at the same level of accuracy as the old version. Or, if it didn't, it was important to know in what way it differed. In order to fully understand any data you take using a machine, it is important to fully understand the machine itself. In other words, if you do not know the machine's reproducibility capabilities, as mentioned before, you will not be able to accurately analyze the noise in your data and thus your data. Thus, I began to analyze this new form of the machine. I took spectra at a default setting of 64 scans with a resolution of 4 wavenumbers. This setting was chosen because it was shown in earlier tests that 64 scans tends to be a setting with minimal noise. This minimal noise means that problems in the data or the new machine would be easier to see since there should be less outside noise.

I began with basic background scans such as the one shown in Figure 17. The one shown in Figure 17 was taken before the Nicolet technicians came and made sure the machine was running properly in its new form. It was taken in the default setting and after I rechecked the alignment of the detector and the mid-infrared source which were not permanently affixed to anything because of the machine and vacuum box's temporary location.

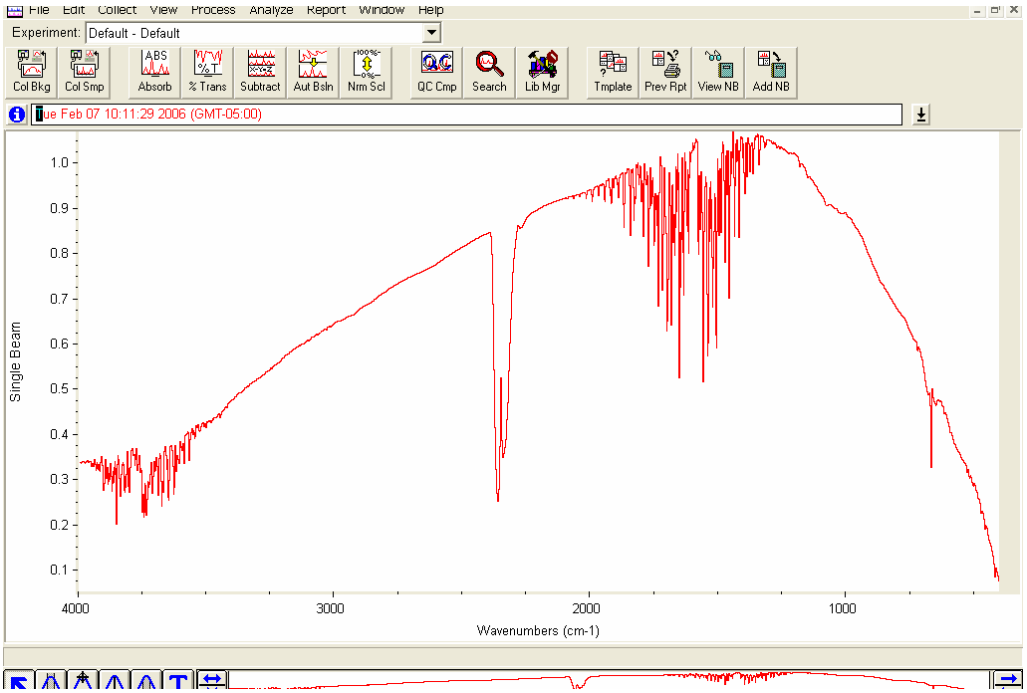

Figure 17. Image showing a background scan taken before the Nicolet technicians adjusted the new configuration of the spectrometer, at 64 scans and a resolution of 4 wavenumbers.

I took several of these backgrounds one after another. The purpose of this was to allow me to then see if the machine was stable by comparing these backgrounds. If the machine was working properly, the backgrounds taken close together in time, with identical settings should look almost exactly the same. These backgrounds could be compared both visually and by analyzing their percent transmission through OMNIC by dividing one background by the other and seeing how close to unity (1) the line is.

Figure 18 shows two consecutively taken backgrounds. The spectra shown in dark blue was taken 15 minutes before the one shown in red. You can see by glancing at the two that they are not quite the same.

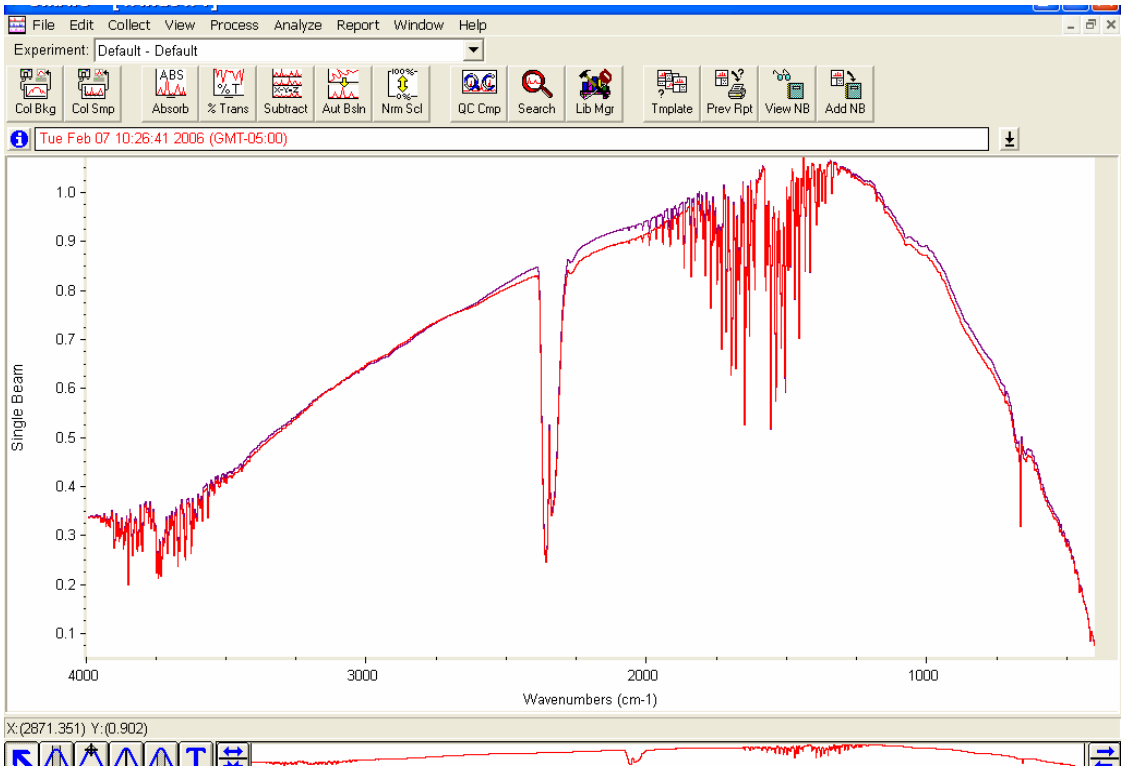

Figure 18. Image showing two consecutively taken backgrounds where the dark blue background was taken 15 minutes before the red one.

Though there isn't a huge disparity between these two spectra, there is a somewhat noticeable difference which could have been due to either the machine or the outside environment. I noticed that a person walking by the apparatus while in the process of taking the 64 scans would hugely and visibly alter the spectra during its measuring and the end result would be an unusually shaped background. In order to try to counter this, we built a makeshift shield around the mid-infrared source using tinfoil at first and then a large plastic bin. The results of these shelters can be seen in Figure 19. A

background taken with the tinfoil is shown in Figure 19 (a) and Figure 19 (b) is a background taken with the plastic bin shelter.

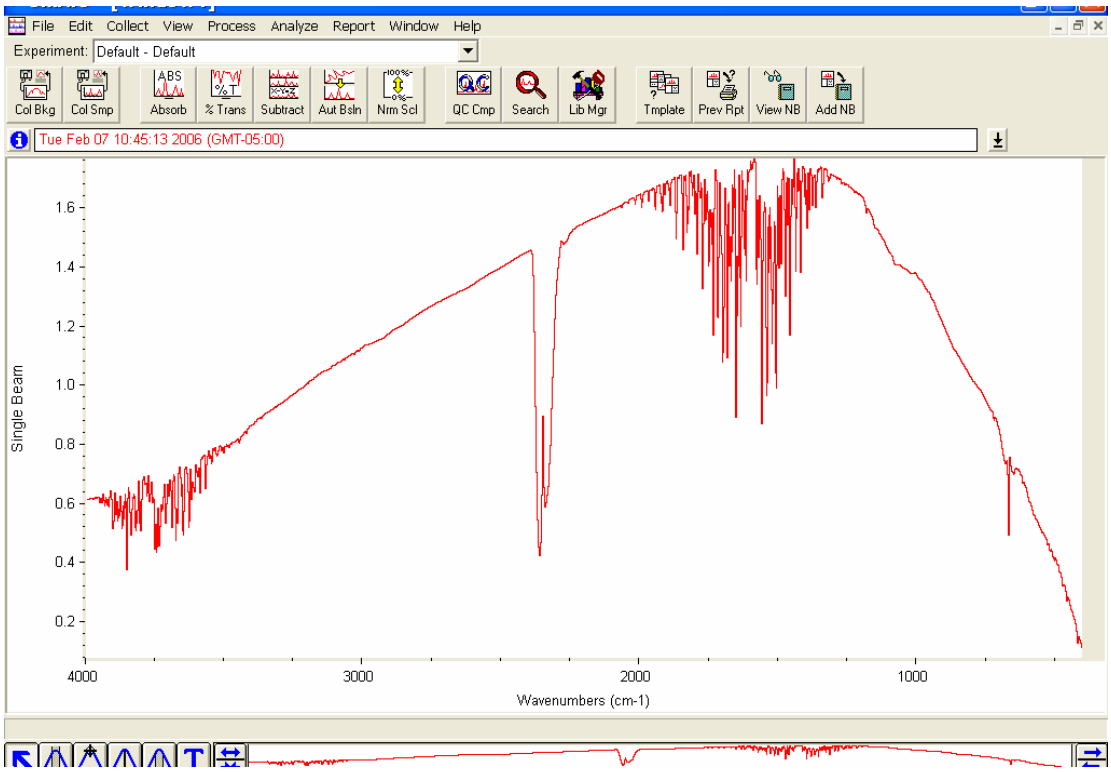

(a)

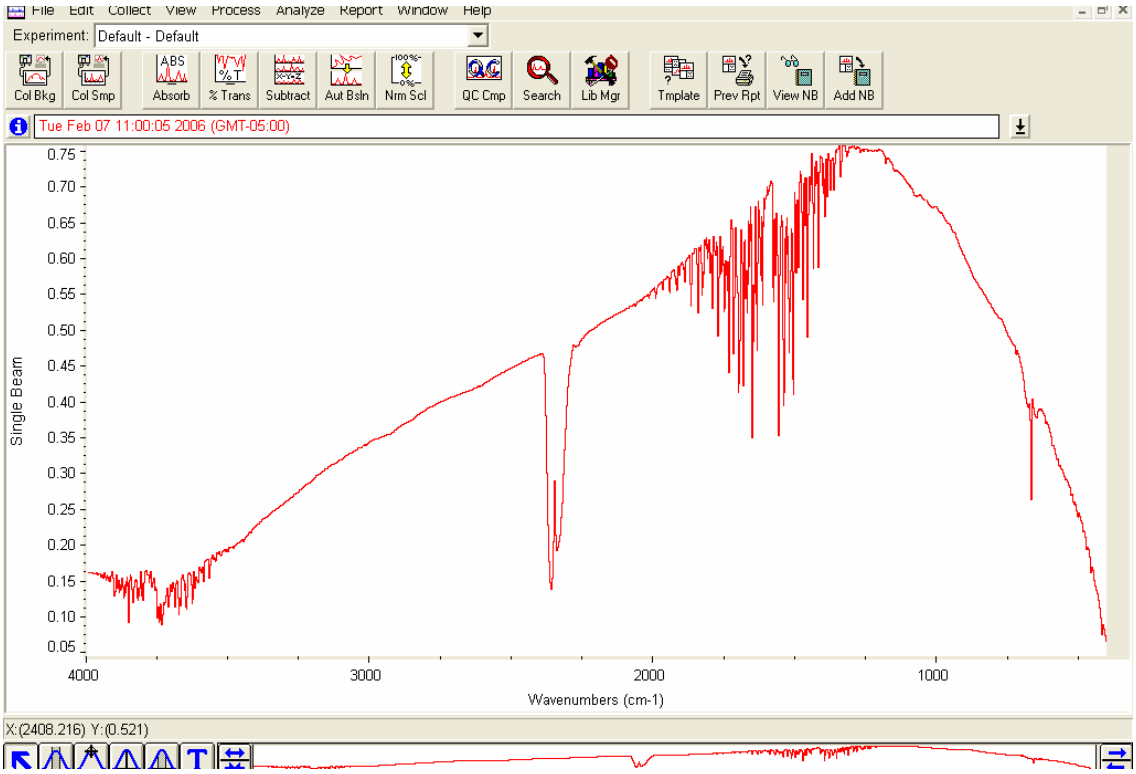

(b)

Figure 19. Images showing background spectra taken with makeshift shelters over spectrometer mid-infrared source. Background in (a) was taken with a tinfoil shelter around the source, and (b) was taken with a plastic bin as a shelter.

The background spectra taken with the plastic bin shelter is actually much further from the appearance of the typical background spectra taken before the spectrometer was moved to its new location. This could be due to other interfering environmental influences such as the source being too insulated by the sturdier shelter and heating up too much. Or, perhaps, this was due to increased air currents around the source because of the hole in the top of the plastic bin acting as a chimney and creating cross currents. There are any number of possible explanations which will no doubt be fixed or at least diminished when the machine is in vacuum.

In order to get further insight into what was going on, however, I reprocessed several of the background spectra to see the percent transmission. Figure 20 shows the

percent transmission, or the ratio of two background spectra taken with the Nicolet in its new location. You can see that the line is not a straight line at all but looks much more like a sinusoidal wave. Studying the interferogram, however, revealed that there was more than one peak (where there should be only one). This meant that the machine was not properly latching onto the peaks and valleys of the alignment laser. In other words, the alignment laser is imbedded in the Michelson interferometer in such a way that it basically is an interferometer within the larger THz interferometer spectrometer. If the machine is working properly, this alignment laser has a sinusoidal signal with noticeable peaks and valleys which can then be compared with the signal being measured. If the alignment laser signal were too weak, the machine would not be able to find it and latch onto it and thus the machine would have trouble taking accurate spectra.

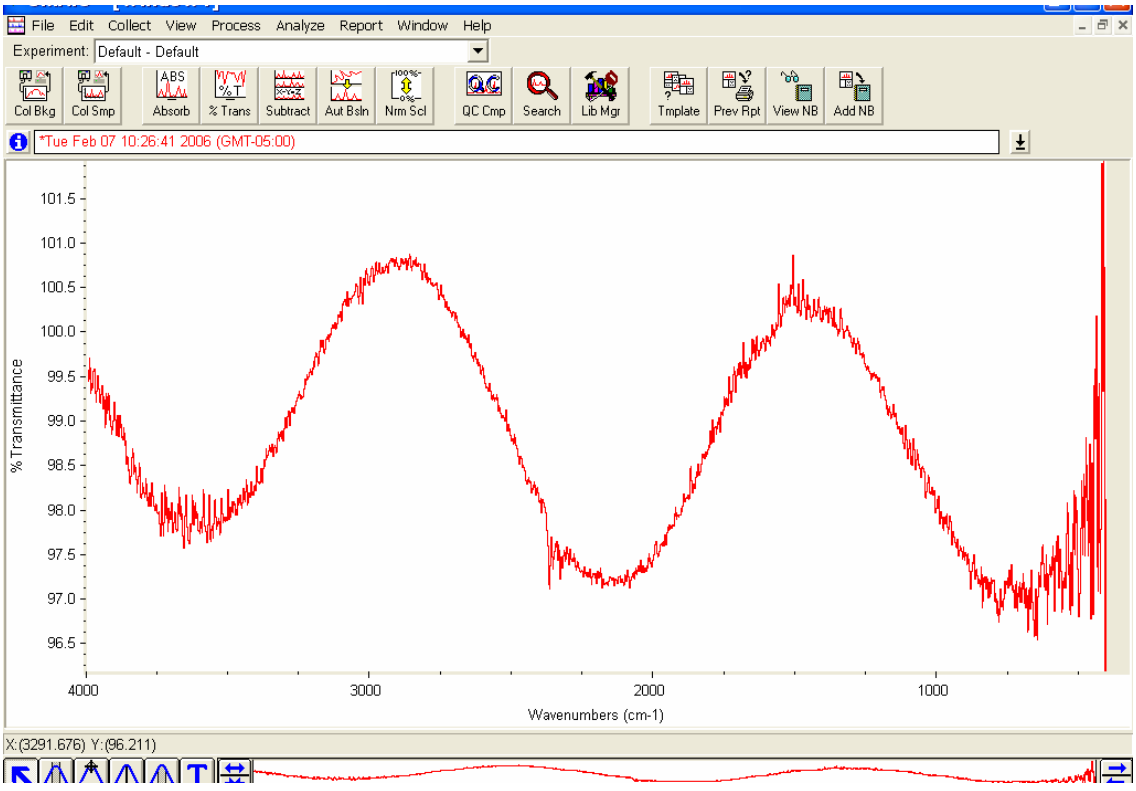

Figure 20. Image showing the percent transmission taken with the Nicolet in its new configuration. Note it's sinusoidal shape due to a weak reference laser signal.

This lack of intensity of the alignment laser and generally irregular and irreproducible spectra made it clear that something was wrong with the machine. Without a strong reference laser signal it is hard for the machine to track the position of the movable mirror. This lack of intensity in the reference laser was likely due to it not being properly aligned and thus loosing a lot of the laser light before it reached the detector. Because of the above tests, the Nicolet technicians were called in to realign the machine and make sure it was running properly after the move. The Nicolet technicians came and showed us how to measure the reference laser signal and set the alignment properly. Once this was done, the reproducibility seemed much improved.

3.4. Using a Frequency Analyzer to Examine the Spectrometer Component Noise

Due to the worse performance of the Nicolet Spectrometer in its new location, it was decided to use a frequency analyzer to study the different individual potential sources of noise. This was done by feeding the signal from the machine into the microphone input of a laptop computer and by using a frequency analyzer program to analyze the noise. The frequency analyzer computer program used was True RTA. All components were turned off except for the desired isolated one.

First five samples of data were taken with just the detector on, with the moveable mirror stationary. Then, five with just the reference laser on (which meant the scanning mirror shown in Figure 7 was able to scan) were taken, then five with only the mid-infrared source on. Finally I took five still frames of data with everything on. Figure 21 shows an example of five samples taken. The graph specifically shows the five taken with just the detector on. It was made from a series of data points taken by the computer

program used to pick up the noise of each component. The x-axis in Figure 21 is the Frequency in Hertz and the y-axis is Signal Amplitude in dBU.

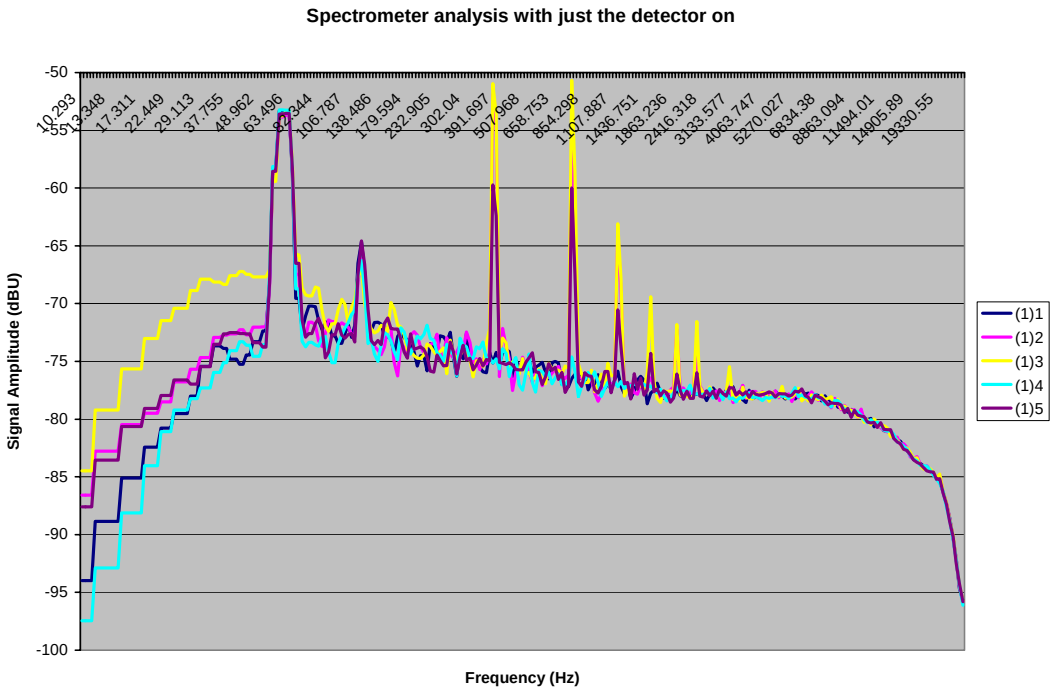

Figure 21. Graph showing five samples taken while the detector was on, but the moveable mirror was stationary and everything else was off.

After the initial 5 samples were taken for each setting, I averaged the y-axis values at each data point on the x-axis. This gave me a single approximate line for each component and one with everything on that I could then easily compare to each other. Figure 22 shows the line of averaged points for each of the settings. The dark blue line labeled (1)average represents the data taken when just the detector was on. The pink line labeled (2)average is the average of the data taken with just the reference laser on (and thus the machine was scanning as well). The yellow line labeled (3)average is from when just the mid-infrared source was on and the turquoise line labeled (4)average represents the average of the data taken with everything on. Again the x-axis is the Frequency in Hz and the Signal Amplitude is in dBU.

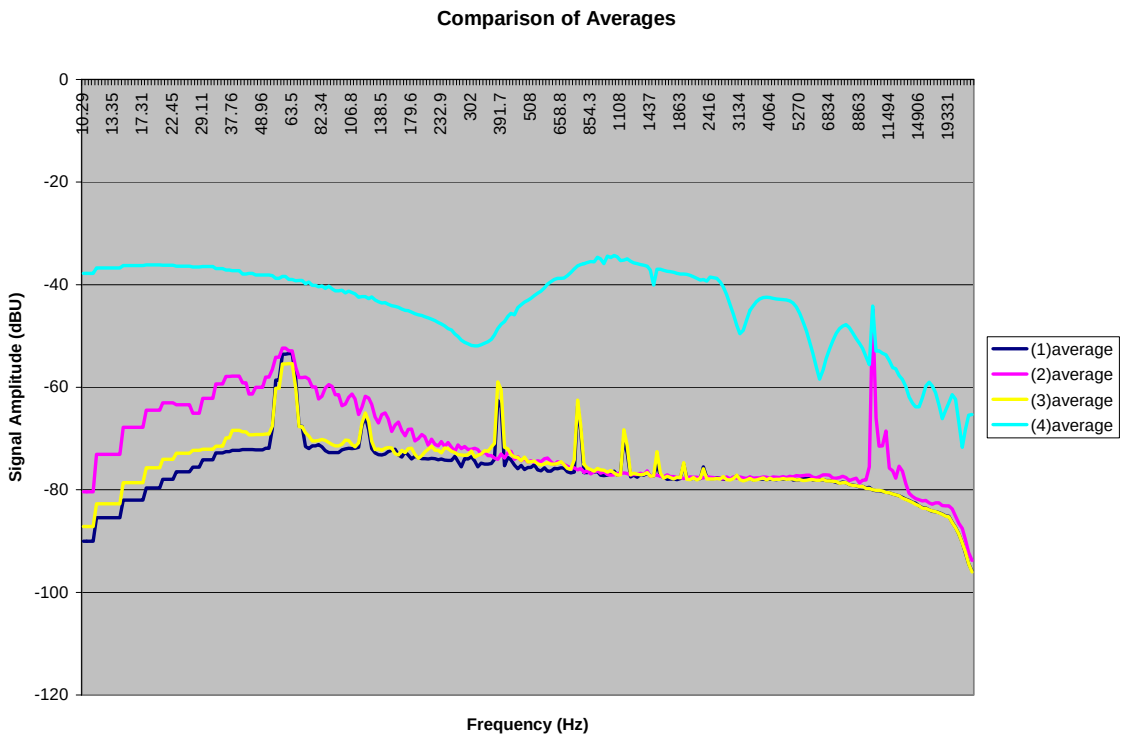

Figure 22. Graph showing the line of averaged points for each setting tested. The dark blue line was taken with only the detector on (the moveable mirror stationary), the pink was with only the reference laser on (and moveable mirror scanning), the yellow was with only the mid-infrared source on and the turquoise was taken with everything on.

4. Conclusions

This research project focused on the commissioning and characterization of high-power THz light. During my research, I leaned how THz light is generated in an electron accelerator. I helped to assemble, install and align the mirrors for the THz beam transport from the FEL vault to the lab so it can be studied. I assisted in the modification, testing and characterization of an FTIR spectrometer. This will eventually help enable users to perform spectral measurements of the THz light in Vacuum.

In addition, I carried out noise measurements on the modified FTIR. This was the process of characterizing the spectrometer for THZ beam measurements. It was first

done by examining the spectra from the Nicolet machine itself and then using a frequency analyzer to separate the noise of the individual components of the machine. The analysis with the frequency analyzer showed that signal to noise is complicated and involves several peaks at specific frequencies. Note that the signal to noise is given by the difference in Fig. 22 between the pink and turquoise curves. This type of analysis is going to play a critical role in what will immediately follow in the FEL THz project, when the THz beam is analyzed.

Overall the experience of working at Jlab showed me a glimpse of the research that goes on at a large physics lab. I gained insight into the manner in which cutting edge physics research is conducted and the importance of a good research team. I learned that large scale research depends on a group of hard working people from a range of backgrounds and experiences. This experience has been "eye-opening" and has no doubt greatly effected my ability to work in groups and apply problem solving skills in all manner of practical situations.

Works Cited

[1] George R. Neil and Gwyn P. Williams, "Evolution of the High Power THz Source Program at Jefferson Lab", *Infrared Physics & Technology* **45**, 389 (2004).

[2] G.L. Carr, M.C. Martin, W.R. McKinney, K. Jordan, G.R. Neil and G.P. Williams "High Power Terahertz Radiation from Relativistic Electrons", *Nature* **420** 153-156 (2002).

[3] Gwyn P. Williams, "Filling the THz gap—high power sources and applications", *Rep. Prog. Phys.* **68**, 1 (2005).

[4] Gwyn P. Williams, "High Power THz Synchrotron Sources", *Phil Trans. R. Soc. Lond*. A **362**, 403 (2004)

Figures:

[Figure 1] G.P. Williams, "Filling the THz gap—high power sources and applications", *Rep. Prog. Phys*. **68**, 4 (2005).
[Figure 2] courtesy of Gwyn P. Williams
[Figure 3] courtesy of TeraView Ltd.
[Figure 4] ibid.
[Figure 5] ibid.
[Figure 6] ibid.
[Figure 10] courtesy of Gwyn Williams
[Figure 11] modified from G.P. Williams, "Filling the THz gap—high power sources and applications", *Rep. Prog. Phys*. **68**, 17 (2005).
[Figure 12] (a) ibid.
[Figure 13] (a) courtesy of Michael Klopf
(b) courtesy of Gwyn Williams from calculations by Paul Dumas, Oleg Chubar and Gwyn Williams
[Figure 14] courtesy of Larry Carr at Brookhaven